
This is an electronic reprint of the original article.
This reprint may differ from the original in pagination and typographic detail.

Author(s): Valkealahti, S. & Schou, J. & Nieminen, Risto M.
Title: Energy deposition of keV electrons in light elements
Year: 1989
Version: Final published version

Please cite the original version:

Valkealahti, S. & Schou, J. & Nieminen, Risto M. 1989. Energy deposition of keV electrons in light elements. *Journal of Applied Physics*. Volume 65, Issue 6. 2258-2266. ISSN 0021-8979 (printed). DOI: 10.1063/1.342839.

Rights: © 1989 American Institute of Physics. This is the accepted version of the following article: Valkealahti, S. & Schou, J. & Nieminen, Risto M. 1989. Energy deposition of keV electrons in light elements. *Journal of Applied Physics*. Volume 65, Issue 6. 2258-2266. ISSN 0021-8979 (printed). DOI: 10.1063/1.342839, which has been published in final form at <http://scitation.aip.org/content/aip/journal/jap/65/6/10.1063/1.342839>.

All material supplied via Aaltodoc is protected by copyright and other intellectual property rights, and duplication or sale of all or part of any of the repository collections is not permitted, except that material may be duplicated by you for your research use or educational purposes in electronic or print form. You must obtain permission for any other use. Electronic or print copies may not be offered, whether for sale or otherwise to anyone who is not an authorised user.

Energy deposition of keV electrons in light elements

S. Valkealahti, J. Schou, and R. M. Nieminen

Citation: *Journal of Applied Physics* **65**, 2258 (1989); doi: 10.1063/1.342839

View online: <http://dx.doi.org/10.1063/1.342839>

View Table of Contents: <http://scitation.aip.org/content/aip/journal/jap/65/6?ver=pdfcov>

Published by the [AIP Publishing](#)

Articles you may be interested in

[Fabrication of nickel diffractive phase elements for x-ray microscopy at 8 keV photon energy](#)

J. Vac. Sci. Technol. B **30**, 031205 (2012); 10.1116/1.3700440

[Electron Transfer in p-Ar Collisions at keV Energies](#)

AIP Conf. Proc. **1099**, 184 (2009); 10.1063/1.3120010

[Calculations of stopping powers of 100 eV – 30 keV electrons in 31 elemental solids](#)

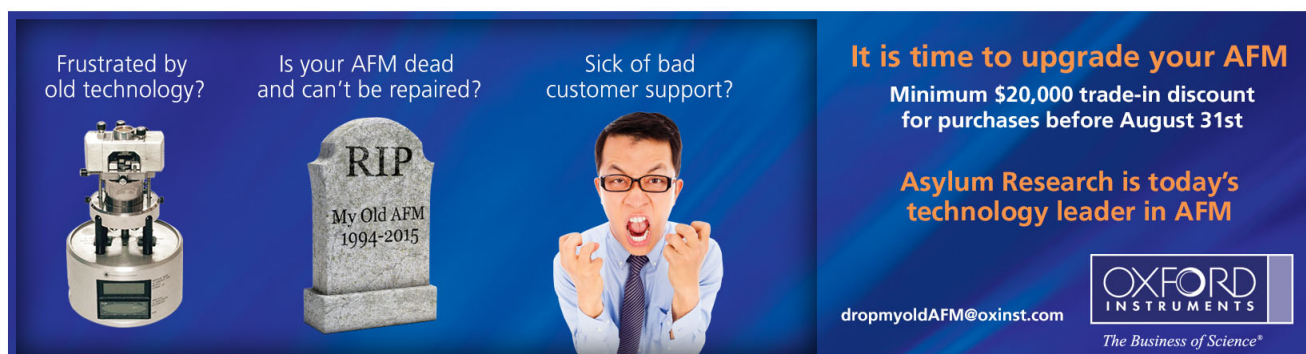
J. Appl. Phys. **103**, 063707 (2008); 10.1063/1.2891044

[Monte Carlo model for the deposition of electronic energy in solid argon thin films by keV electrons](#)

J. Appl. Phys. **80**, 5653 (1996); 10.1063/1.363617

[New elastic electron scattering factors for the elements for incident energies of 10, 40, 60, and 90 keV](#)

J. Chem. Phys. **85**, 6810 (1986); 10.1063/1.451417



Frustrated by old technology? Is your AFM dead and can't be repaired? Sick of bad customer support?

It is time to upgrade your AFM

Minimum \$20,000 trade-in discount for purchases before August 31st

Asylum Research is today's technology leader in AFM

dropmyoldAFM@oxinst.com

OXFORD INSTRUMENTS
The Business of Science®

The advertisement features three panels: an old AFM, a tombstone for 'My Old AFM 1994-2015', and a frustrated man. The background is dark blue with light blue accents.

Energy deposition of keV electrons in light elements

S. Valkealahti

Department of Physics, University of Jyväskylä, SF-40100 Jyväskylä, Finland

J. Schou

Association EURATOM-Risø National Laboratory, Physics Department, DK-4000 Roskilde, Denmark

R. M. Nieminen

Laboratory of Physics, Helsinki University of Technology, SF-02150 Espoo, Finland

(Received 28 September 1988; accepted for publication 21 November 1988)

The Monte Carlo simulation method has been used to investigate the spatial distribution of deposited energy for 1–10 keV electrons incident on solid hydrogen, nitrogen, neon, silicon, aluminum, and argon. In the simulation, elastic scattering cross sections are calculated exactly using the single-atom crystalline potentials. Inelastic energy loss processes for hydrogen are based on the ionization cross section from Green and Sawada [J. Atmos. Terr. Phys. **34**, 1719 (1972)] and the gas-phase stopping power from Parks *et al.* [Nucl. Fus. **17**, 539 (1977)]. For the heavier materials a modification of Gryziński's [Phys. Rev. A **138**, 305 (1965); **138**, 322 (1965); **138**, 336 (1965)] semiempirical expression for each core and valence electron excitation is used. The energy-deposition distribution of keV electrons and the ionization distribution of weakly bound electrons are practically equal, whereas the penetration depth distribution extends deeper into the material than the energy-deposition distribution. The energy-deposition distributions of keV electrons for light materials, except for hydrogen, can be represented quite well by a universal distribution. In addition, accurate Gaussian approximations for the different materials in the entire energy region from 1 to 10 keV have been evaluated. Parameters such as the mean penetration depth and the mean energy-deposition depth are included as well.

I. INTRODUCTION

The irradiation of solids by charged particles in the keV regime results in a large number of electronic excitation and ionization processes in the solid. The spatial distribution of the energy that is deposited in the solid by keV electrons is governed by the energy dissipation and scattering processes. For electron energies below 10 keV this energy distribution is considerably influenced by the generation of high-energy secondary electrons and the subsequent production of excitations or ionizations.

The spatial distribution of deposited energy plays an important role in atmospheric physics^{1,2} as well as in hole-electron pair generation in semiconductors.^{3,4} As another example, the distribution of luminescence centers in insulators is determined by this distribution.^{5,6} Recently, it has been demonstrated that the value of the distribution at the surface is important for the secondary electron emission^{7,8} as well as sputtering of frozen gases.^{9,10} A related aspect, which has been discussed frequently in the literature, is the spatial distribution of x-ray emission in connection with electron probe microanalysis.^{11,12}

The measurements have been performed predominantly for insulating materials and gases with primary electron energies from about 4 keV up to 80 keV.^{2,13,14} Everhart and Hoff³ determined the charge-carrier generation in a system of aluminum, silicon dioxide, and silicon bombarded by 6–20-keV electrons. The only measurements so far for metals have been carried out by Cosslett and Thomas¹⁵ who evaluated the spatial distribution of deposited energy for gold and copper by an indirect method.

The distribution of deposited energy has been determined theoretically by Spencer^{16,17} for several elements and chemical compounds for primary electron energies of 25 keV or above. For water irradiated by electrons of a few keV the distribution has been calculated by Gupta and Prasad¹⁸ and Turner *et al.*¹⁹ Recently the energy dissipation profile was estimated for 30 keV electrons in copper by Fathers and Rez.²⁰

A large number of Monte Carlo (MC) calculations for metals, semiconductors, and insulators have been reported in the literature. Berger and Seltzer computed the distribution of 2–10-keV electrons incident on atmospheric air with and without high-energy secondaries.¹ Since the energy-loss distribution of the primaries did not deviate significantly from the complete distribution, the former was calculated in most of the cases. A similar energy-loss distribution was computed by Bishop²¹ for several metals at 30 keV, Shimizu, Honji, and Murata²² for aluminum and copper at 30 keV, Matsukawa, Murata, and Shimizu²³ for several metals at 10 keV, and more recently by Kotera, Murata, and Nagami²⁴ for gold at 10 keV. For several semiconductors general expressions for the energy-loss distribution were suggested by Barbier *et al.*²⁵ on the basis of MC calculations. Murata, Kyser, and Ting²⁶ included high-energy secondaries in their study of bulk polymethylmethacrylate samples irradiated by 10- and 20-keV electrons. The secondaries were included as well in the computations by Grosswendt and Waibel²⁷ for 0.3–3-keV electrons incident on nitrogen and by Heaps and Green²⁸ for electrons with energies up to 2 keV on hydrogen.

In the present work extensive MC simulations are reported for a number of light insulators ($1 < Z < 18$), with pri-

primary electron energies between 1 and 10 keV. The presentation includes aluminum and silicon for completeness. In all cases the high-energy secondaries are included. The simulated depth distributions for the deposited energy are presented together with suitable Gaussian approximations.

II. THE DISTRIBUTION OF DEPOSITED ENERGY

In the following treatment we concentrate on perpendicular incidence and on the one-dimensional depth distribution of deposited energy. The general form of the distribution in a material, which is bombarded by keV electrons, is known from the literature, as described in the Introduction. The distribution has a pronounced maximum around one-third of the experimentally determined range (Fig. 1). The peak is caused by a combination of electron scattering and slowing-down processes. The shape is similar for all materials, but the absolute magnitude depends strongly on the material.

The starting point for most of the theoretical considerations is the energy-deposition distribution $D(E, x, \cos \alpha)$ resulting from irradiation by primary electrons of energy E with the angle of incidence α . It is determined by the sum of the average kinetic energy of all electrons located in a depth element $(x, x + dx)$ after both the primary and secondaries have slowed down below a certain energy limit (cutoff energy), which is very small compared to the initial energy.

The equations that govern the analogous distribution of energy deposited in electronic excitations and ionizations for ion slowing-down have been described comprehensively by Winterbon²⁹ and Schou.⁷ A similar system of equations for electron incidence alone was obtained by Schou,⁷ but the treatment has not yet been refined to a level, from which feasible predictions emerge.

Most of the existing measurements of the distribution rely on luminescence rather than an evaluation of the kinetic energy. The spatial distribution of luminescence centers reflects the distribution of ionized atoms or molecules. However, Winterbon, Sigmund, and Sanders³⁰ have shown for a

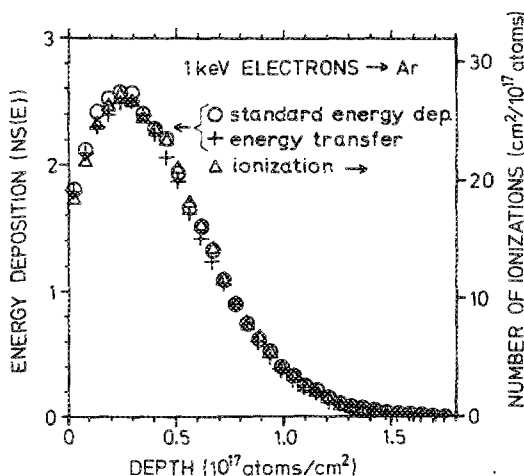


FIG. 1. Ionization profile of the least bound electrons, energy transfer profile, and the standard energy-deposition profile as a function of depth for 1-keV electrons incident on argon. The profiles have been normalized to have the same area.

related problem that the spatial distribution of damage centers, which in this context correspond to ionizations, is equivalent to the theoretical distribution of deposited kinetic energy apart from normalization.

The inelastic scattering cross section, which will be utilized for almost all elements, is a modified version of Gryziński's ionization cross section.³¹ For a target electron shell denoted by i the differential ionization scattering cross section is

$$\frac{d\sigma_i(E, \Delta E)}{d(\Delta E)} = \frac{\pi e^4 N_i}{(\Delta E)^3} \frac{E_{B_i}}{E} \left(\frac{E}{E + E_{B_i}} \right)^{3/2} \left(1 - \frac{\Delta E}{E} \right)^{E_{B_i}/(E_{B_i} + \Delta E)} \times \left[\frac{\Delta E}{E_{B_i}} \left(1 - \frac{E_{B_i}}{E} \right) + \frac{4}{3} \ln \left[2.7 + \left(\frac{E - \Delta E}{E_{B_i}} \right)^{1/2} \right] \right], \quad (1)$$

where N_i , ΔE , E_{B_i} , and E are the number of electrons in shell i , the energy loss of the incident electron, the mean electron binding energy in shell i , and the primary projectile energy, respectively.

We do not utilize details of the cross section, but treat it as a model cross section which enables us to determine the sum of all energies which are lost within a certain depth interval. For instantaneous projectile energies which are larger than the corresponding binding energy, $\Delta E - E_{B_i}$ is the kinetic energy of the secondary (unless it is larger than the energy of the primary, cf. Sec. III). In the standard simulation E_{B_i} (for $\Delta E > E_{B_i}$) and ΔE (for $\Delta E < E_{B_i}$) have been registered at each depth, i.e., the energy used to ionize (binding energy) or excite an electron to a bound state is counted into the distribution. The kinetic energy of an electron after it has slowed down below the cutoff energy of the simulation is sampled as well. The paths of all secondaries are followed separately and their energy losses are also counted.

The spatial distribution of energy transfer ΔE is shown in Fig. 1 for 1-keV electrons on argon together with our *standard* distribution of binding and excitation energy. Apparently, the two distributions deviate very little from each other. Therefore, in the following we consider only the standard distribution.

It is possible also to determine the number of ionization events in shell i within a certain depth interval. Such a distribution is also shown in Fig. 1. Only the ionizations from the shell with the lowest binding energy have been included in the ionization distribution. Actually, this combination of energy and element shows the largest disagreement between the three distributions.

III. PRESENTATION OF THE METHOD

A. Monte Carlo simulation method

The Monte Carlo simulation is a widely used and commonly approved method to investigate in detail the slowing down of charged particles in matter. Also a large number of useful MC calculations of the electron energy-loss properties in different materials have been reported by other authors as described in the Introduction.

The Monte Carlo simulation method has been used to study the energy deposition of 1–10-keV electrons normally incident on light materials. The MC simulation program was originally developed for keV electron and positron slowing down calculations by Valkealahti and Nieminen.^{32,33} Later the inelastic energy loss procedure was improved particularly for keV electron penetration calculations in the hydrogen-gold system.³⁴ Here, we describe only the main features of the present MC simulation procedure, as the details have been presented earlier.^{32–35}

The interaction processes between 1–10-keV electrons and matter are predominantly of two types. The electrons scatter elastically from atomic Coulomb potentials or inelastically from core and valence electrons. Furthermore, the inelastic processes can be divided into ionization and excitation.

The elastic scattering process is calculated on the basis of the effective single-atom potential in condensed matter. It is evaluated as follows: First, a free-atom potential and electron density are calculated self-consistently by the density-functional method.^{36–38} Second, an approximative crystal-line charge density and Coulomb potential are obtained by superimposing atomic charge densities and potentials in a lattice. The spherical average of the charge density and Coulomb potential around a given atom are then evaluated. Third, the exchange and correlation effects between electrons are accounted for by adding a local-density-dependent exchange-correlation potential³⁸ to the Coulomb potential.

The phase shifts of an electron scattered from the effective crystalline central potential are obtained by numerically solving³⁹ the radial Schrödinger equation. The differential scattering cross section is then calculated from the partial wave sum⁴⁰ and the total elastic scattering cross section is obtained by integrating over the angles.

For nitrogen, neon, aluminum, silicon, and argon the inelastic collisions are described separately for each electron level on the basis of Gryziński's excitation function³¹ for ionization processes [Eq. (1)]. For each material all contributing electron levels are included.^{41,42} The excitation

TABLE I. Ratio of the threshold energy E_{th} , to the binding energy E_{B_i} for contributing shells i and the mean excitation energy I (see Refs. 44–46).

Material	E_{th}/E_{B_i}	I (eV)
N ₂	0.72	88
Ne	0.81	137
Al	0.77	163
Si	0.76	173
Ar	0.65	190

processes (bound-bound transitions) are included by using a constant approximation for the low-energy differential scattering cross section (Fig. 2). The value of that cross section is equal to the differential ionization scattering cross section [Eq. (1)] for $\Delta E = E_{B_i}$. The threshold energies E_{th_i} associated with each shell i are chosen so that the ratio E_{th_i}/E_{B_i} is constant for all contributing electron shells i in a material and the total electronic stopping power is equal to the Bethe result⁴³ at 10 keV. The ratios E_{th_i}/E_{B_i} and the mean excitation energies I , used in the Bethe formula, are presented in Table I.

For hydrogen the inelastic scattering model is based on the total stopping power expression from Parks, Turnbull, and Foster⁴⁷ and the ionization cross section from Green and Sawada.⁴⁸ A constant excitation cross section between the threshold energy $E_{th} = 8.8$ eV and the ionization energy $E_B = 15.42$ eV is utilized so that the total stopping power is equal to the expression by Parks and co-workers.⁴⁷ The whole differential inelastic scattering cross section is then multiplied by the constant $C = 0.75$, which includes a possible reduction of the stopping power from gas phase to solid hydrogen. The reduction of the stopping power by a factor of 0.75 resulted from the fit of the simulation that showed the best agreement with the experimental electron reflection measurements on the hydrogen-gold system.³⁴

Trajectories of 10 000 incident electrons are calculated in each simulation and a termination energy of 20 eV is applied. Both the paths of the primary electron and all secondary electrons are followed. The contributions from the secondaries are included in all calculated parameters and distributions unless otherwise noted.

B. Feasibility of the simulation method

There are two types of basic experimental data, which can be used for an appropriate test of the simulation procedure at keV energies. First, the transmission probabilities through thin films have been measured for several materials. The transmission probabilities of electrons and positrons through thin aluminum and copper films were simulated^{32,35} and good agreement was found with the experimental transmission data.^{49–52} Second, the backscattering probabilities from numerous semi-infinite solids have been measured for keV electrons. The backscattering probabilities have been compared^{33–35} with experimental results for several materials and good general agreement is found, as shown in Fig. 3 for argon, aluminum, nitrogen, and hydrogen.^{51–58} Both the transmission and backscattering probabilities of electrons of

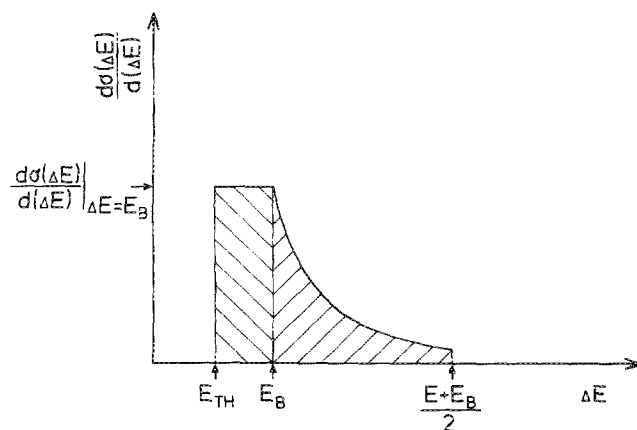


FIG. 2. Schematic drawing of the differential inelastic scattering cross section used in the present approach. The shaded area under the curve to the right of E_B is the Gryziński's ionization cross section (or the Green and Sawada cross section for hydrogen) and the shaded area to the left of E_B is the excitation cross section.

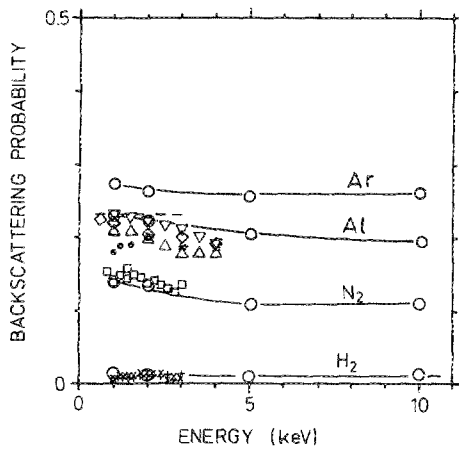


FIG. 3. Reflection coefficient as a function of energy for electrons normally incident on hydrogen, nitrogen, aluminum, and argon. Circles are Monte Carlo results and the solid lines are drawn just to guide the eye. Both the primary and secondary electron reflections are counted with the cutoff of 50 eV, which corresponds to the experimental grid voltage. Experimental data: +, H₂, Risø (Ref. 53); ×, D₂, Risø (Ref. 53); □, N₂, Risø (Ref. 54); ▽, Al, Vyatskin *et al.* (Ref. 52); ◇, Al, Fitting (Ref. 55); △, Al, Vyatskin and Khranov (Ref. 51); ●, Al, Roptin (Ref. 56); *, Al, Bronstein and Denisov (Ref. 57); ---, Al, Thomas and Pattinson (Ref. 58).

the present MC simulation model^{34,35} with the improved inelastic scattering cross section are in better agreement with the experimental data than the results of the earlier simulations.^{32,33}

In addition to the direct ways of checking the validity of the MC results, some indirect but convincing experimental results have been reported. For example, Vehanen *et al.*⁵⁹ have recently confirmed that the shape of the positron implantation profile is well approximated by a derivative of a Gaussian function, in agreement with the MC simulations.^{32,33,35} They measured the annihilation line-shape parameter⁶⁰ as a function of positron implantation energy in multilayer structures of Al₂O₃, Al₂O₃/ZnS, Al₂O₃, or Al₂O₃/ZnS/Al₂O₃ grown on a glass substrate. Those measurements were very sensitive to the shape of the positron implantation profile and only by using the profiles indicated by the MC simulations could the experimental annihilation line-shape parameter versus the incident energy curves be reproduced.

Moreover, the penetration depth properties of electrons (and positrons) in solids can be compared to some direct experimental results. For example, the median penetration depth has been deduced from several thin-film transmission measurements^{49-51,61} and the behavior as function of energy is similar to that of the calculated mean penetration depth. The behavior is expected to be similar, because the range profile of keV electrons has practically the same shape independent of the material and energy.³⁵ The shape of the range profile of keV electrons in the very light materials (e.g., hydrogen) differs slightly from the general shape.

The simulation procedure demonstrates the importance of the inelastic scattering cross section. The present adjustment of the threshold value E_{th} is crucial for the precise agreement between the simulated and experimental data for the reflection coefficients from the solids in Fig. 3. The re-

sults from Ref. 34 show that an increase of the electron stopping power via a change of E_{th} leads to a clear reduction of the backscattering yield.

IV. RESULTS

The present standard distribution of deposited energy incorporates the energy loss to all electron shells for both primaries and secondaries as well as the termination energy of the moving electrons. As mentioned previously (Fig. 1) this distribution is very similar to the spatial distribution of ionizations from the outermost electron shell. Even the ionization distribution of the tightly bound inner-shell electrons did not deviate much from the standard distribution. This agreement was found from calculations of the ionization distributions of all electron shells. All the calculated distributions are qualitatively similar, but the ionization distribution of a tightly bound electron level is slightly nearer to the surface than the ionization distribution of the least bound electrons. The reason for this is that electrons have lost a part of their energy when they have penetrated deeply into the material and the remaining energy is not sufficient to ionize the tightly bound electrons.

Since the depth scale is important for the scaling properties of the standard distribution, we have to consider a suitable length unit for the comparisons between different primary energies and materials. The standard concept is the range r_0 determined by the intercept of the extrapolation of the linear part of the distribution on the right-hand side of the maximum with the horizontal axis, $D(E, x, 1) = 0$ (Fig. 4).^{1,2} We have not used this extrapolated range, even though a well-defined quantity has been suggested by Everhart and Hoff³:

$$r_0 = \alpha_0 E^{1.75}, \quad (2)$$

where the primary energy E is in keV and $\alpha_0 = 4 \mu\text{g}/\text{cm}^2$. However, Eq. (2) is an approximation only for $10 < Z < 15$, and a practical determination of r_0 requires either a subjective estimate or a complicated procedure after the simulation. This extrapolated range is different from the usual range concepts as for example the mean penetration depth r (Fig. 5) and the mean path length. The range distribution is always deeper in the material than the energy-deposition dis-

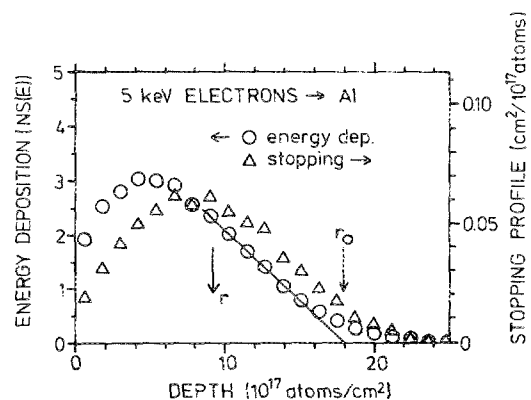


FIG. 4. Penetration depth profile of primary electrons and energy-deposition profile of 5-keV electrons incident on aluminum.

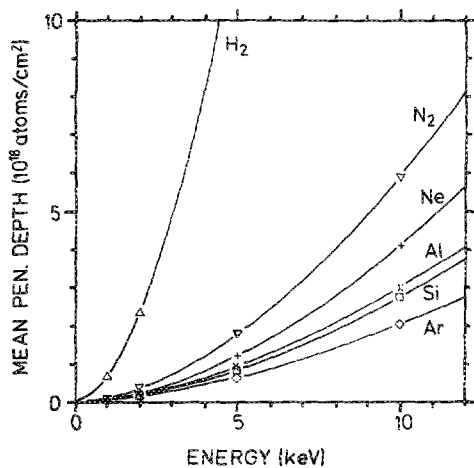


FIG. 5. Mean penetration depth as a function of electron energy. The solid curves show the range approximation from Table II.

tribution, because the range distribution is a sampling of the termination points, whereas the energy-deposition distribution includes points from the entire trajectory. Therefore, the mean energy-deposition depth r_E is always smaller than the mean penetration depth. Since both quantities must be calculated, and in fact are quite similar apart from a constant ratio, we have decided to use r_E as the unit for the depth scale in the comparisons.

The mean energy-deposition depth r_E for a semi-infinite target is described well by the approximation

$$r_E = \alpha E^n, \quad (3)$$

where E is the incident energy in keV, and n and α are constants, characteristic for each material (Table II). Also the mean penetration depth r may be approximated by a relation similar to Eq. (3). r_E is about 20% smaller than r for all primary energies considered here. For the mean energy-deposition depth at 1 keV α is well approximated by 61×10^{16} atoms cm^{-2}/Z except for hydrogen. This relationship is demonstrated in Fig. 5 and in Table II as well. Essentially, the dependence on the atomic number reflects that the stopping power is proportional to the atomic number of the target material in this energy region.

The distribution of deposited energy is depicted in units of the stopping power $NS(E)$ rather than in the normalized

TABLE II. Parameters of the exponential fit, Eq. (3), to r and r_E vs incident energy data. The exponent n is a unitless constant and α is given in units of 10^{16} atoms/cm².

Material	r		r_E	
	n	α	n	α
H ₂	1.81	66.9	1.81	48.8
N ₂	1.73	10.9	1.74	8.6
Ne	1.74	7.5	1.74	5.9
Al	1.70	6.0	1.70	4.8
Si	1.70	5.5	1.70	4.3
Ar	1.65	4.9	1.65	3.6

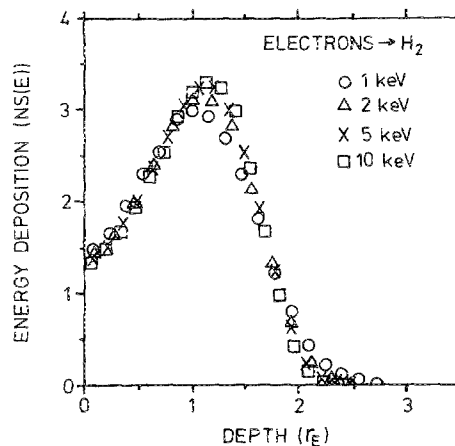


FIG. 6. Standard energy-deposition profiles of 1-, 2-, 5-, and 10-keV electrons incident on hydrogen. The depth is given in units of the mean energy-deposition depth and the energy deposition in units of the stopping power.

units which, for example, Grün,² Berger and co-workers,¹ and Everhart and Hoff³ have applied. The reason is the obvious advantage that the energy-deposition density at the surface $D(E,0,1)$ up to $NS(E)$ is produced by the incoming electrons, whereas the exceeding value $D(E,0,1) - NS(E)$ is caused by backscattered or secondary electrons.^{7,8,22} As a matter of fact, the step $NS(E)$ at the surface was utilized by Grün² for the experimental determination of the stopping power. In the present work the values of the stopping power are obtained from Gryziński's cross section [Eq. (1)] as described previously.

The existing data for the energy deposition of keV electrons in solid hydrogen are scarce. In Fig. 6 the energy-deposition profile is presented for 1-, 2-, 5-, and 10-keV electrons in the lightest element, solid hydrogen, and in Fig. 7 similar profiles for a heavier material, silicon, are shown. The distributions for solid hydrogen between 1 and 10 keV are quite similar in units of r_E and $NS(E)$, whereas the distributions for silicon deviate more from each other. The values close to the maximum increase as a function of the primary energy. The increase is more pronounced for silicon and argon than

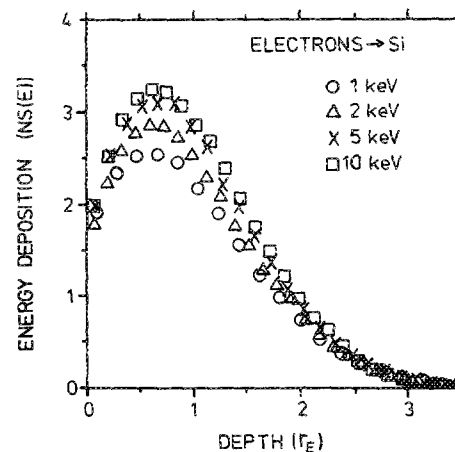


FIG. 7. Standard energy-deposition profiles of 1-, 2-, 5-, and 10-keV electrons incident on silicon.

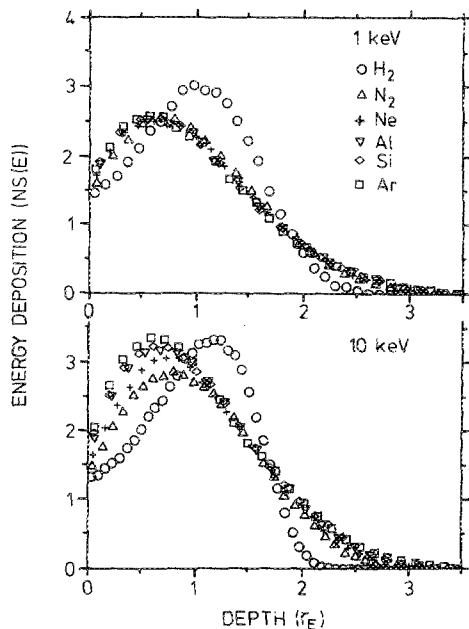


FIG. 8. Standard energy-deposition profiles of 1- and 10-keV electrons.

for solid hydrogen but occurs also for heavier materials such as copper at considerably higher energies.¹⁷ This shape dependence on the primary energy is, of course, suppressed, if the energy-deposition profile is approximated by a standard polynomial, as, for example, the one from Everhart and Hoff.³ On the other hand, Fig. 6 shows that the distribution in hydrogen for energies between 1 and 10 keV may be approximated by an average curve in the present units. Actually an average curve is feasible for silicon as well, but the deviations are much larger for silicon than hydrogen.

The possibility of having one "universal" curve for all light materials is demonstrated by the curves in Fig. 8. Only the distribution for hydrogen deviates strongly from those of the others both at 1 and 10 keV. The distributions for the other elements ($7 < Z < 18$) are similar apart from depths less than r_E at 10 keV. This similarity means that it would be possible to approximate the energy-deposition distribution for these elements by the neon or aluminum curves with an acceptable accuracy. Consequently, the present units, r_E and $NS(E)$, allow us to evaluate one simple curve in analogy to the standard curve from the work of Grün² or Everhart and Hoff.³ However, rather than offer an average distribution we prefer to present approximations for all elements in the present energy region, in such a way that the features of the individual distributions are significant (Sec. VI).

The most striking difference for the distributions in different elements is illustrated in Fig. 8 for 10 keV. If we disregard solid hydrogen, one notes that with rising atomic number the maximum value increases and the position shifts towards the surface. The reason for both effects is the enhancement of the backscattering probability with the atomic number, which means that the fraction of energy absorbed near the surface is enhanced. Both trends have been demonstrated by Spencer in the computations¹⁷ as well.

Furthermore, the surface value $D(E, 0, 1)$ increases with the atomic number for the energies under consideration.

Even the value for hydrogen fits into this pattern. The increase is caused, again, by the increasing backscattering probability of electrons with the atomic number of the elements.

V. COMPARISONS TO PREVIOUS RESULTS

We have compared our Monte Carlo simulations to some of the most relevant experimental and theoretical results of other authors as well as to other MC simulations.

In Fig. 9 the energy-deposition distribution of 5-keV electrons in nitrogen is compared with experimental and theoretical distributions in air. The MC distribution agrees well with the luminescence radiation measurements by Grün² for 5-keV primary electron energy in air. In the surface region our simulated values are slightly lower than others. Our results are also in good agreement with the fluorescence measurements by Cohn and Caledonia⁶² for 2–5-keV electrons in nitrogen gas (not shown in the figure). These kinds of measured profiles are very accurate estimates of the real energy-deposition distributions and should be considered as the most relevant data for comparison. The theoretical evaluation by Spencer¹⁷ for above 25-keV energies differs slightly from the profiles of other authors at lower energies. However, it seems to be a general trend (Figs. 6 and 7 and Ref. 2) that the profile becomes sharper and moves deeper into the material with increasing energy.

Numerous Monte Carlo simulations have been performed to investigate the energy deposition of electrons in different materials. Berger and co-workers¹ have made a MC

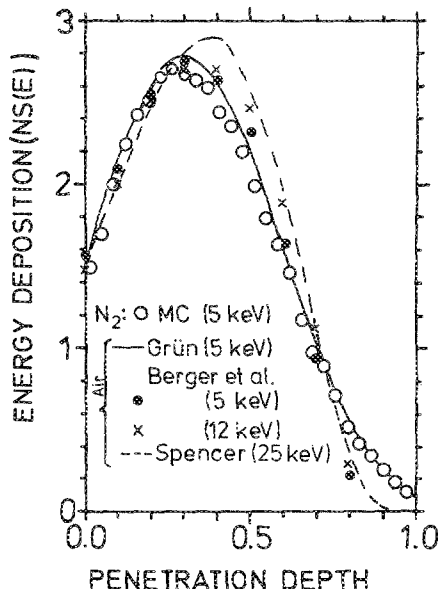


FIG. 9. Standard energy-deposition distribution of 5-keV electrons in solid nitrogen and air along the surface normal. The energy deposition is plotted in units of the stopping power and the depth in units of the practical electron range r_p from Berger and co-workers (Ref. 1). Our Monte Carlo distribution for 5-keV electrons in nitrogen is plotted so that nitrogen has the same surface density (in units of g/cm^2) as air in the experimental distribution from Grün (Ref. 2) for 5-keV electrons. The dashed line is a theoretical curve from Spencer (Ref. 17) and the crosses and circles are from the Monte Carlo calculations by Berger and co-workers (model B in Ref. 1) for air.

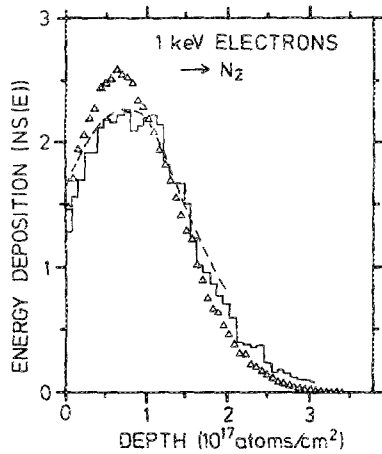


FIG. 10. Standard energy-deposition profile of 1-keV electrons incident on nitrogen. The triangles denote our Monte Carlo calculations, the histogram Monte Carlo results from Grosswendt and Waibel (Ref. 27), and the dashed line experimental data from Barrett and Hays (Ref. 13).

calculation for air where the elastic collisions are handled on the basis of the screened Rutherford cross section including a spin-relativistic correction factor. The inelastic collisions are treated by the continuous-slowing-down approximation. Their results are in good agreement with our results. Only the decreasing tail deep in the material is missing from their distribution. The obvious reason is that they have used the continuous-slowing-down approximation to describe the inelastic energy losses instead of the Monte Carlo sampling, which is superior, and a simulation cutoff energy of 200 eV compared to ours of 20 eV.

For 1-keV electrons incident on nitrogen the experimental and Monte Carlo energy-deposition distributions of Barrett and Hays¹³ and Grosswendt and Waibel,²⁷ respectively, are in satisfactory agreement with our MC simulations (Fig. 10). Both of them are somewhat more spread out in nitrogen than our distribution. Their ranges are also about 10% larger than ours and the experimental ranges by Grün² and Cohn and Caledonia.⁶² Grosswendt and Waibel²⁷ have used the screened Rutherford scattering cross section for elastic collisions in their MC calculations. The Rutherford cross section underestimates considerably the elastic collisions at keV energies³³ and therefore increases the penetration. In addition to this reduction, Grosswendt and Waibel diminished the cross section by a factor of 0.65 in order to obtain an agreement with electron backscattering data on molecular nitrogen below 100 eV. This procedure is responsible for the low energy-deposition values compared to our results at small depths.

Our energy-deposition profiles in aluminum and silicon are in qualitative agreement with the experimental data by Everhart and Hoff³ for aluminum-silicon dioxide-silicon multilayer target (Fig. 11). Our mean energy-deposition depth is about 10% larger than their depth, but the distributions have the same shape. Everhart and Hoff evaluated the energy-deposition profiles indirectly from the measured charge-carrier generation in the layer of silicon dioxide as a function of the incident electron energy. Furthermore, the authors presented an energy-independent expression which

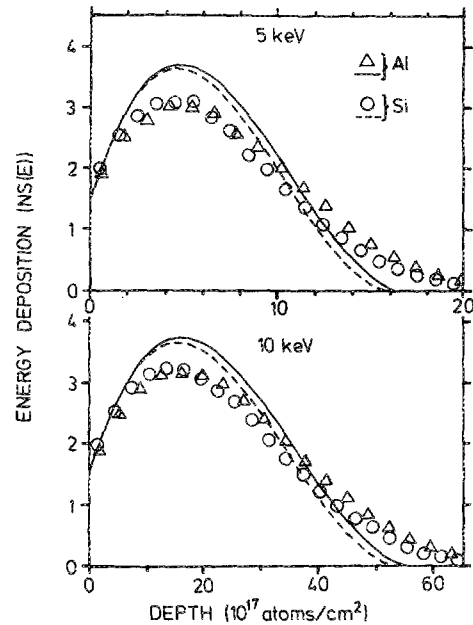


FIG. 11. Standard energy-deposition profile of 5- and 10-keV electrons incident on aluminum and silicon. The triangles and circles are MC values for aluminum and silicon, respectively. The solid and dashed lines indicate the Everhart-Hoff profile for aluminum and silicon, respectively, derived from the experimental aluminum-silicon dioxide-silicon data by Everhart and Hoff (Ref. 3).

was supposed to cover the entire energy region from 5 to 25 keV. Therefore, our curve for 10 keV agrees better with the Everhart-Hoff profile than that for 5 keV.

VI. GAUSSIAN APPROXIMATION

The standard energy-deposition distributions of electrons in the studied materials have quite a similar shape. The distribution differs slightly from those for heavier materials only for hydrogen. Therefore, we present a parametrization which primarily agrees with the distributions for heavier materials. However, this parametrization can be a useful approximation also for hydrogen in many applications. Of course, a more accurate profile for hydrogen can be obtained by using Fig. 6 and Tables II and IV.

We approximate the energy-deposition distribution of normally incident electrons by a Gaussian profile, written as

$$D(E, x, 1) = AG(E, x), \quad (4)$$

TABLE III. Parameters of the exponential fit, Eqs. (3) and (4), to r_G and σ_G vs incident energy data. The exponent n is a unitless constant and α is given in units of 10^{16} atoms/cm².

Material	r_G		σ_G	
	n	α	n	α
H ₂	1.83	47.8	1.78	29.3
N ₂	1.78	6.5	1.71	6.6
Ne	1.80	4.2	1.71	4.8
Al	1.75	3.3	1.66	4.1
Si	1.74	2.9	1.70	3.5
Ar	1.66	2.5	1.67	2.9

TABLE IV. The stopping power $NS(E)$ (above), the stopping cross section (middle), and the surface value of the energy-deposition distribution $D(E,0,1)$ of the Gaussian fit (below) for 1-, 2-, 5-, and 10-keV electrons. $NS(E)$ and $S(E)$ are given in units of eV atoms/Å and eV cm²/10¹⁵ atoms, respectively, and $D(E,0,1)$ in the stopping power units [$NS(E)$]. The values of D for hydrogen close to the surface deviate so much from the MC simulation that they are not included in the table.

Energy	H	N	Ne	Al	Si	Ar
1 keV	0.2335	1.084	1.447	2.231	1.930	1.234
	0.4391	2.448	3.109	3.701	3.862	4.599
		1.572	1.736	1.836	1.899	1.893
2 keV	0.1384	0.673	0.902	1.425	1.243	0.814
	0.2603	1.520	1.939	2.364	2.488	3.033
		1.543	1.776	1.836	1.927	2.017
5 keV	0.0671	0.341	0.461	0.739	0.650	0.434
	0.1263	0.770	0.991	1.227	1.300	1.617
		1.477	1.739	1.947	2.041	2.095
10 keV	0.0384	0.198	0.270	0.436	0.384	0.259
	0.0722	0.446	0.579	0.723	0.768	0.966
		1.464	1.681	1.950	2.078	2.241
Atomic density (Å ⁻³)	0.053	0.044	0.047	0.060	0.050	0.027

where

$$G(E,x) = (1/\sqrt{2\pi\sigma_G^2}) \exp[-(x-r_G)^2/2\sigma_G^2]. \quad (5)$$

$r_G(E)$ and $\sigma_G(E)$ are the mean depth and the standard deviation of the distribution. $A(E)$ is a material-dependent parameter that varies approximately as the primary energy. $A(E)$ is fixed by the normalization

$$\int_0^\infty D(E,x,1) dx = E - E_r, \quad (6)$$

where E_r is the average energy that is carried away by the reflected electrons. $r_G(E)$ and $\sigma_G(E)$ are given in Table III, and $A(E)$ may be determined from Table IV through the relation $D(E,0,1) = AG(E,0)$. The Gaussian approximation can be applied for many distributions other than the standard energy-deposition profile just by introducing a proper constant A (rescaling). It was pointed out in Secs. I and II that, for example, the ionization, excitation, and energy-transfer distributions are practically all similar. The stop-

ping power $NS(E)$ and the surface value of the energy-deposition profile $D(E,0,1)$ are presented in Table IV for all the studied energy and material combinations. A Gaussian distribution has been suggested previously for electron probe microanalysis at energies around 30 keV by Wittry.⁶³

The mean depth and the standard deviation of the Gaussian distribution increase as functions of energy similarly to the mean energy-deposition depth [Eq. (3)]. Parameters of the fits of Eq. (3) to the r_G and σ_G versus incident energy data are presented in Table III. Both for r_G and σ_G the power n decreases slightly as a function of atomic number of the target material similarly as for r and r_E , but is practically the same in a given material for all the four parameters (Tables II and III). The value of α for both quantities depends more strongly on the material. The mean depth r_G is about $0.8r_E$ except for hydrogen.

Apart from hydrogen, the Gaussian approximation describes the energy-deposition and associated profiles of keV electrons in the studied materials, as well as in heavier materials,³⁴ very well (Fig. 12).

The agreement between the Gaussian approximation and the MC simulation demonstrates that it is possible to use the scaling procedure

$$D(E,x,1) = (E/r)\lambda(x/r) \quad (7)$$

for an individual material, as long as the requirements of accuracy are not too large. r is usually an extrapolated range, e.g., that from Everhart and Hoff [Eq. (2)], and λ a dimensionless function of the ratio x/r alone. If the exponent n in the expression for this r is close to that for r_E and r_G , it means that λ is almost independent of the primary energy E . However, this feasibility of λ for one material does not mean that one may apply this material-dependent λ for other elements than neighbor elements with a fair accuracy. The variation of the exponent n with the atomic number is obviously so strong (Tables II and III), that a "universal" expression for λ cannot exist, even not for the lightest elements. Therefore,

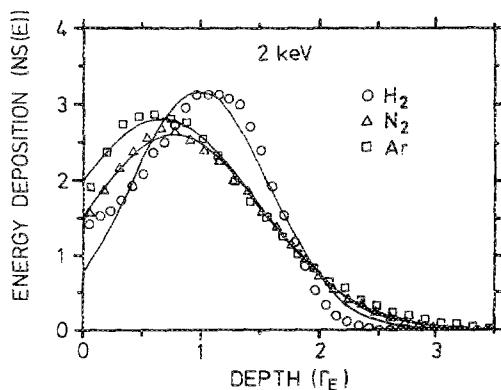


FIG. 12. Standard energy-deposition profile of 2-keV electrons incident on hydrogen, nitrogen, and argon. The solid lines are fits of the Gaussian profile to the MC distributions.

